JOURNAL OF GEOPHYSICAL RESEARCH, VOL. 95, NO. A12, PAGES 20,997-21,005, DECEMBER 1, 1990

Path-Dependent Properties of Subionospheric VLF Amplitude and Phase Perturbations Associated With Lightning

T. G. WOLF AND U. S. INAN

Space, Telecommunications And Radioscience Laboratory, Stanford University, Stanford, California

A comprehensive study of lightning-associated amplitude and phase perturbations on multiple VLF/LF signals (Trimpi events) observed at Stanford, California and at Palmer Station, Antarctica, has revealed a number of new properties that appear to be characteristic of the particular signal paths. (1) Signal amplitude changes are on the whole evenly distributed between enhancement and attenuation, but some individual signal paths have strong preferences for one or the other. (2) Phase changes on almost all paths show a strong preference for advancement, with phase retardation occurring rarely. (3) The range in size of amplitude and phase changes appears to be relatively constant for a given path, but it is found to vary between different paths. None of the existing models of the Trimpi effect are found to explain all of the observed new features. Instead, the new experimental findings provide an empirical framework to guide the evaluation of more sophisticated models. Analysis also indicates that the magnitudes of simultaneous amplitude and phase changes are only weakly correlated and that the recovery signatures of amplitude and phase events can be substantially different, with the signal amplitude generally recovering faster. This apparent independence of amplitude and phase perturbations is interpreted to result from the altitude distributed nature of the ionospheric disturbances.

1. INTRODUCTION

The Trimpi effect consists of transient perturbations, caused by lightning, in the amplitude or phase of VLF (3-30 kHz) and LF (30-300 kHz) radio signals propagating in the Earth-ionosphere waveguide. The majority of observed events are believed to be due to wave-induced precipitation of radiation belt electrons, a process involving a series of atmospheric interactions, as follows. VLF impulses generated by lightning propagate along magnetic field lines into the magnetosphere, where they undergo cyclotron resonance with trapped energetic electrons. The resulting pitch angle scattering of the electrons causes some of them to precipitate into the ionosphere, either directly, or after mirroring or backscattering in one hemisphere. These precipitating electrons disturb the ionosphere, causing localized ionization enhancements in the vicinity of the VLF reflection height in the ionosphere and thus perturb the propagation of subionospheric VLF signals. The enhanced ionization then decays back to normal ambient levels as a result of recombination and attachment [*Helliwell et al.*, 1973].

Trimpi events have been observed on signals at frequencies as low as 3.79 kHz from the transmitter at Siple Station, Antarctica [*Carpenter et al.*, 1985], and at frequencies as high as 780 kHz from a broadcast transmitter at Santa Cruz, Argentina [*Carpenter et al.*, 1984]. In addition to the changes in amplitude originally observed [*Helliwell et al.*, 1973], advances in the phase of the received signal [*Lohrey and Kaiser*, 1979] and delays in phase [*Inan et al.*, 1985] have been found, as well as simultaneous changes in amplitude and phase on a single signal [*Inan and Carpenter*, 1987; *Dowden and Adams*, 1988]. Most reported observations involve amplitude changes ranging from 0.04 dB [*Carpenter et al.*, 1984] to 6 dB [*Helliwell et al.*, 1973] and show phase changes as large as 12° [*Inan and Carpenter*, 1987].

Analysis of the time signature of observed events has added support to the mechanism described above [*Inan and Carpenter*, 1986], as well as revealing additional information. The typical event onset takes 0.1-2 s, and recoveries resemble exponentials and last for 10-100 s [*Carpenter et al.*, 1984]. Some low-latitude events with initially rapid recovery signatures were interpreted as involving particularly high-energy electrons (~1 MeV) [*Inan et al.*, 1988*a*]. Analysis of time delays between the lightning discharge and the signal perturbations revealed the involvement of both northbound and southbound whistlers [*Inan and Carpenter*, 1986].

A relatively small subset of observed Trimpi events were found to display temporal features not consistent with whistler-induced electron precipitation from the magnetosphere. Such events, referred to as early/fast Trimpi events, involve signal changes that occur within <50 ms of the causative lightning discharges or radio atmospherics and are believed to be due to direct upward coupling of lightning energy to the lower ionosphere [*Armstrong*, 1983; *Inan et al.*, 1988*b*; *c*].

Trimpi events have been observed in the Antarctic [*Hurren et al.*, 1986; *Inan and Carpenter*, 1987], New Zealand [*Lohrey and Kaiser*, 1979; *Dowden and Adams*, 1988; 1989], and in the northern hemisphere from Stanford University in California; Lake Mistissini, Quebec; Saskatoon, Saskatchewan; and Arecibo, Puerto Rico [*Inan et al.*, 1988*a*; *b*; *c*; *d*; 1990; *Burgess and Inan*, 1990; *Yip et al.*, 1990]. In attempts to localize and estimate the size of the disturbance in the ionosphere, events have been correlated with detected lightning strokes [*Inan et al.*, 1988*b*] and simultaneous events on multiple paths (even to different receiving sites) have been identified [*Inan et al.*, 1990]. Research on the theoretical aspects of this phenomenon has progressed in parallel with experimental results. The whistler-electron interaction in the magnetosphere has been modelled, identifying the energy distribution and flux levels of precipitating electrons [*Chang and Inan*, 1985], and these findings have been supported by satellite observations of precipitating electrons correlated with whistlers observed on the ground [*Voss et al.*, 1984; *Inan et al.*, 1989]. The propagation of signals in the Earth-ionosphere waveguide including the effect of localized ionospheric disturbances has been modeled [*Tolstoy et al.*, 1982] and the sensitivity of various signal paths to this phenomenon has been explored [*Tolstoy et al.*, 1986]. More recently, disturbed regions located off the direct signal path have

Paper number 90JA01766.
0148-0227/90/90JA-01766$05.00

been considered [*Dowden and Adams*, 1988; 1989], and a full three dimensional model for the location of disturbance in the waveguide has been introduced [*Poulsen et al.*, 1990].

Although the distributions in magnitude of VLF signal changes that occur in Trimpi events and the relative distributions of amplitude and phase have been studied [*Tolstoy et al.*, 1986; *Inan and Carpenter*, 1987; *Dowden and Adams*, 1988; 1989], the variation in these distributions with signal path had not yet been investigated. Several models of the effects of the enhanced ionization on the subionospheric signals suggest different variations in these distributions, so the variability or consistency of the distributions would be indicative of the utility of the models. In this paper, we undertake a first comprehensive study of the occurrence rates and magnitudes of signal perturbations (both in amplitude and phase) in propagation data collected from two different sites over extended periods of time. We then discuss our results in the context of different theoretical models of the ionospheric disturbance and its effect on the subionospheric VLF/LF signals.

Some aspects of the data analysis and the criteria for event recognition are discussed in the section 2, which is followed by a separate section on data coverage. The distribution of amplitude and phase perturbations are presented in section 4 and the significance of these results are discussed in section 5. A final section describes the independence of the time signatures of amplitude versus phase Trimpi events.

2. Data Analysis and Event Recognition

A key requirement for our study was to develop a procedure to identify and measure perturbations in a consistent manner. The procedure developed to provide reliable results involved a number of separate steps, beginning with reviewing low-resolution plots of the collected data and ending with the measurement of the size and temporal signature of each event.

First, low time resolution summary plots, generated when the data was collected, were reviewed, and periods of time (typically several hours long) that appeared to have characteristic perturbations (the specific criteria are defined below) in either amplitude or phase were identified. These periods were then replotted at higher resolution, for analysis. This replotting made it possible to recognize events consistently and to measure them with a resolution of 0.1 dB in amplitude and 0.5° in phase. The replotted data points were time-averaged over 0.64 s, in order to provide smoothing of the data and to maximize the consistency of the perturbation magnitude measurements.

In typical received data, other longer term ionospheric and magnetospheric effects cause changes in the measured amplitude and phase of VLF signals. Thus, in most events the signal amplitude or phase does not return to the pre-event levels, but instead returns to a projected level the signal would have reached at that time if the event had not occurred. Taking this effect into account, the criteria for recognizing an event were formulated as follows:

1. Either the amplitude or the phase of the signal has an abrupt change, of at least 0.1 dB or 0.5°, occurring within 2 s.

2. The signal returns to a subjective visually extrapolated pre-event level over a time of 10 to 200 s.

These criteria were found to identify characteristic events consistently, but probably allowed a small fraction of poorly defined events to be left out of the data analyzed. In particular, during periods when the signals exhibited other rapid fluctuations, it was often impossible to recognize a return to pre-event levels. We note, however, that these occurrences were uncommon and appeared with roughly equal frequency on amplitude and phase and on all channels analyzed, so that the statistical results comparing the behavior of different signals would not be expected to be altered by the omission of these questionable events. The size of each of the identified events was determined by manually measuring the magnitude and polarity of the change in both amplitude and phase. It was found that measuring the pre-event and post-event levels and then taking the difference introduced substantial errors, while measuring the pre-event level and the magnitude of the change provided consistent results. Thus, for each event, five quantities were tabulated: the time of occurrence, the pre-event amplitude, the change in amplitude, the pre-event phase, and the change in phase. This table of events was subsequently analyzed for patterns in the relative occurrence of amplitude and phase events on different paths.

Since not all of the events were analyzed at high time resolution, no distinction was made between events which have temporal signatures consistent with whistler-induced electron precipitation or those that are of the early/fast category as discussed above. In most cases that were analyzed, the events were found to be in the former category.

3. Description of Data Coverage

The data used in this analysis were limited to that collected with a newly developed phase/amplitude receiver [*Wolf*, 1990] in order to assure the consistency of the results. This receiver is capable of measuring the signal amplitude and the phase of one sideband of the modulated signal at high time resolution ($\sim$ 20 ms). In this paper, we confine our attention to the analysis of data acquired prior to July 1988 at Stanford University, California and Palmer Station, Antarctica. Table 1 lists the eight signal paths, the frequencies, and the path lengths. Also shown are the months for which data was collected, the number of days for which data was available, the number of hours that had Trimpi activity, and the actual number of events found. The transmitter locations and propagation paths are illustrated in Figure 1.

Owing to Antarctic logistics constraint for data retrograde, the data available from Palmer Station were limited to that from April and May 1988. However, since Palmer Station (65°S, 64°W, L = 2.4) is in a region of very high event activity [*Carpenter and Inan*, 1987], these two months provided substantial quantities of usable data. At Palmer Station, simultaneous amplitude and phase data were collected on four different signal paths, selected for monitoring on the basis of their known characteristics, such as adequate signal strength and substantial perturbation activity. These paths to Palmer Station originated at the NPM transmitter in Hawaii (NPM-PA), the NLK transmitter in Washington (NLK-PA), the NSS transmitter in Maryland (NSS-PA) and the NAA transmitter in Maine (NAA-PA). Because of the high number of events on it, the NPM-PA path was used to study some additional details of event characteristics, for example, the variation of characteristics with time, and the variation of amplitude events with corresponding phase events.

Data have been collected with systems at Stanford University (37°N, 122°W, L = 1.8) since November 1986, but on a sporadic basis, whenever field systems were being developed or tested. As a result, there are many gaps in the collection schedule, but over the year and a half that systems were being developed (November 1986 to July 1988), a reasonable quantity of data had been collected on four signal paths. These paths to Stanford originated at the NLK transmitter (NLK-SU), the 48.5-kHz transmitter in Nebraska (48.5-SU), the NSS transmitter (NSS-SU), and the NAU transmitter in Puerto Rico (NAU-SU). The 48.5-SU path was monitored infrequently because the modulation on this transmitter is often changed several times per night, precluding consistent phase

TABLE 1. Characteristics of the Signal Paths Analyzed

Transmitter	Frequency, kHz	Receiver	Distance, km	Months Analyzed	Total Days	Active Hours	Number Events
NSS	21.4	Stanford	3964	Nov.-May	136	36	141
NAU	28.5	Stanford	5726	March-May	57	19	92
NLK	24,8	Stanford	1220	June-July	44	9	61
48.5	48.5	Stanford	2160	Nov.,July	8	2	15
NPM	23.4	Palmer	12335	May	18	51	578
NLK	24.8	Palmer	13506	May	18	6	33
NSS	21.4	Palmer	11579	April	11	6	28
NAA	24.0	Palmer	12161	April	11	5	22

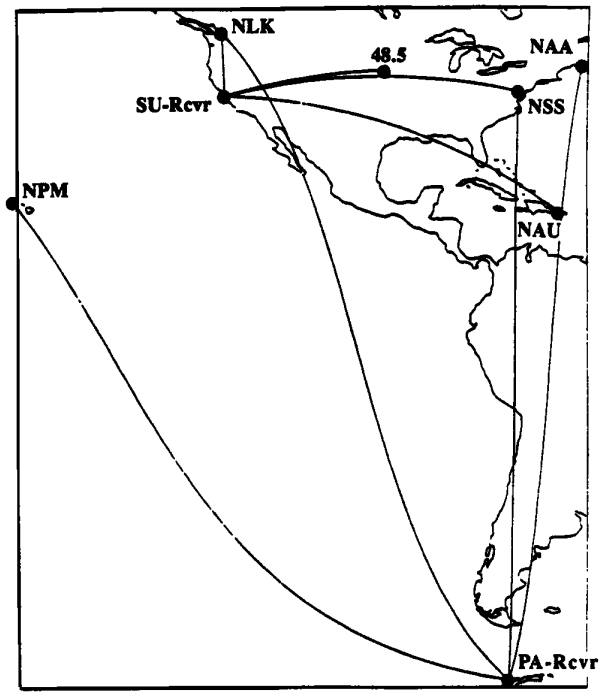

Fig. 1. A map of the western hemisphere, showing the eight signal paths monitored for the data included in this analysis. Four signals were received at Palmer Station, Antarctica (PA-Rcvr), and four were received at Stanford University, California (SU-Rcvr).

measurements. As a result, only 15 events were found during a total of 2 hours of activity, so results for this path may not be statistically significant.

4. Distribution of Amplitude and Phase Perturbations

For each path, the polarity distribution (amplitude enhancement versus attenuation and phase advancement versus retardation) is plotted in Figure 2 (amplitude changes) and Figure 3 (phase changes). From Figure 2 it is clear that different paths have quite different amplitude polarity distributions. The NPM-PA and NLK-SU paths show a strong preference for amplitude attenuation, while NLK-PA data have an equally strong tendency toward amplitude enhancement. For the other paths tendencies were not as strong, but attenuation is more prevalent on NAU-SU, NSS-SU is evenly distributed, and enhancement is more common on 48.5-SU, NSS-PA, and NAA-PA.

The distribution of phase perturbations shown in Figure 3 exhibits a striking asymmetry in the polarity of phase changes. With the exception of 48.5-SU, the other seven paths exhibit a preference for phase advancement (or no measurable phase change). The 48.5-SU path is comparatively short and crosses mountainous land, and the signal has a substantially higher frequency than the others analyzed; all facts that would be expected to substantially increase the number of waveguide propagation modes with significant amplitude and thus complicate the path properties [*Davies*, 1965]. In addition, only a small set of events was available on this

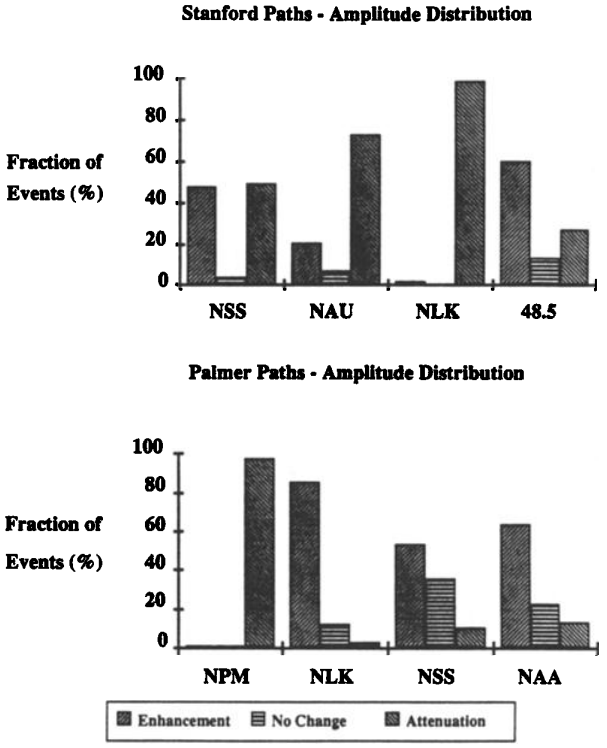

Fig. 2. Signals observed at Stanford (top) and (bottom) signals observed at Palmer Station. For each path the percent of events that had amplitude enhancement, amplitude attenuation, and no amplitude change (only a phase change) are shown.

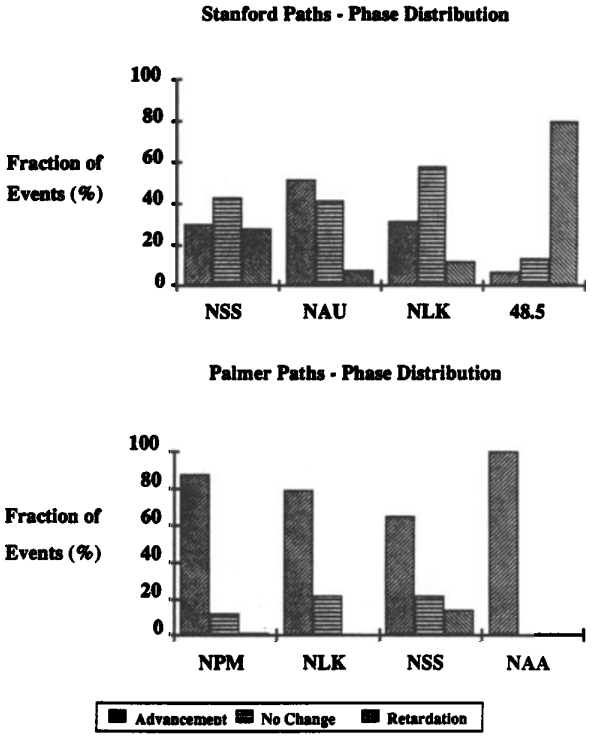

Fig. 3. Signals observed at Stanford (Top) and (bottom) signals observed at Palmer Station. For each path the percent of events that had phase advancement, phase retardation, and no phase change (only an amplitude change) are shown.

path (15 events over 2 hours), so results must be considered to be tentative. The substantially more common occurrence of phase advancement on the other paths, despite the differences between these paths appears to be an important property of the Trimpi phenomenon.

Another important property in characterizing the mechanism of the Trimpi effect is the relative magnitude of simultaneous amplitude and phase changes. Some models suggest that there should be a direct relationship between the size of the phase change ($\Delta\phi$) and the size of the amplitude change (ΔA), while others suggest that large phase changes should coincide with small amplitude changes and vice versa (see section 5).

Figure 4 contains scatter plots of $\Delta\phi$ vs simultaneous ΔA for each of the eight paths investigated. On each graph, a point is plotted for each event investigated, except NPM-PA, which had so many events that only the first 150 are plotted (a similar plot of all 578 events appears the same, but more cluttered). It is obvious that no path shows a strong correlation between ΔA and $\Delta\phi$, either directly or inversely. Instead on each path, while there are a few scattered large events, the majority of events lie in a fairly uniform distribution within a rectangle characterized by some maximum change in amplitude (ΔA_m) and some maximum change in phase ($\Delta\phi_m$). The size of this rectangle (ΔA_m by $\Delta\phi_m$) varies from path to path, as if it were a property of the path. In order to verify this possibility, similar scatter plots were made for the NPM to Palmer path for each day for which more than 10 events were found. These plots, shown in Figure 5, demonstrate that the size of the rectangle enclosing the event distribution does not vary significantly from day to day on a single path.

In addition to the variation in size of this rectangle, these scatter

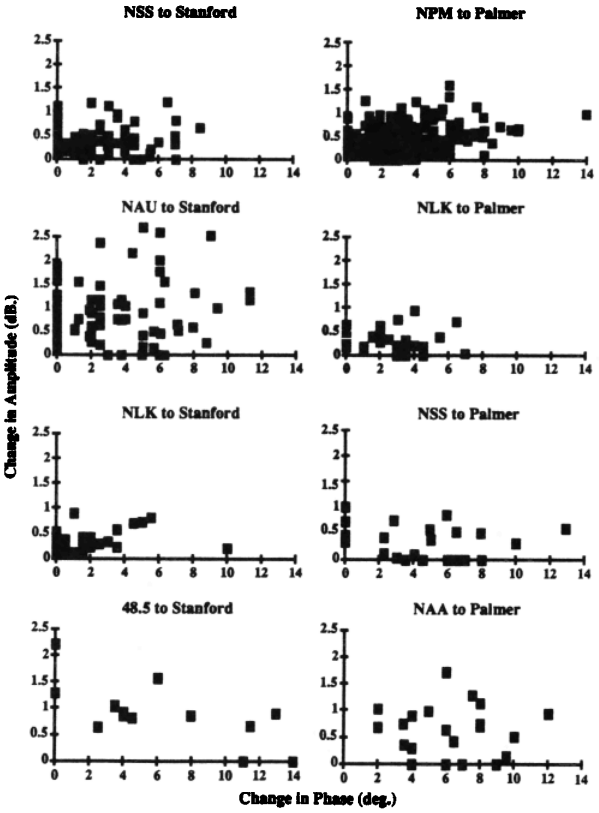

Fig. 4. For each path analyzed, a point is plotted for each event showing the magnitude of the simultaneous amplitude and phase change. For the NPM to Palmer path, only the first 150 events are plotted. A similar plot of all 578 events on this path appears the same, but more cluttered.

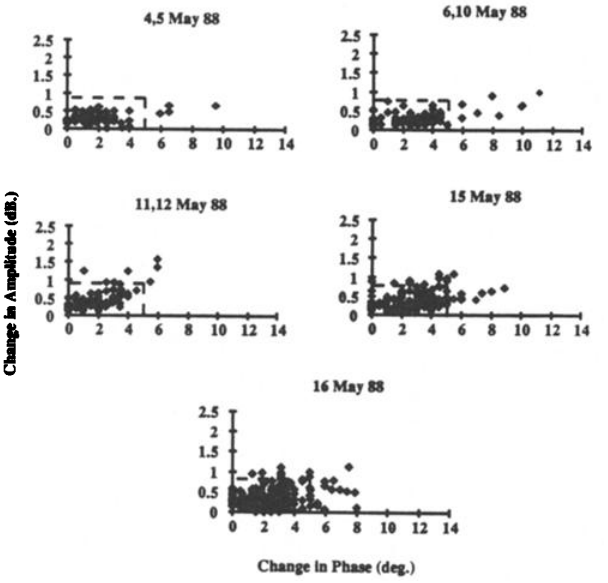

Fig. 5. For the NPM-PA path, a scatter plot of ΔA versus $\Delta\phi$ is shown for each day (or pair of days) for which more than 10 events per day were found. For each day, the majority of events are fairly uniformly distributed within the rectangle of ΔA_m = 0.8 dB and $\Delta\phi_m$ = 5°.

plots (Figure 4) reveal the apparent independence of the magnitude of ΔA and the simultaneous $\Delta\phi$. On all paths studied, the rectangle of ΔA_m and $\Delta\phi_m$ is fairly uniformly filled with events, so the magnitudes could, at best, be weakly correlated. Another illustration of the relatively weak correlation between amplitude and phase events is shown in Figure 6. In this figure the NPM to Palmer events were divided into categories according to the magnitude of ΔA. Within each category the events are sorted according to the magnitude of $\Delta\phi$, and the number of events in each $\Delta\phi$ range are shown. There appears to be a weak correlation between strong amplitude and strong phase events, since small ΔA (~0.1 dB) are most likely to have $\Delta\phi \sim 2°$, and large ΔA (~0.9 dB) are most likely to be associated with $\Delta\phi \sim 4°$. This 2° difference may seem significant, but within any given amplitude category, the spread in observed phase changes is 4°-6°. Thus the magnitude of $\Delta\phi$ is only weakly correlated with the magnitude of ΔA.

Since the range of event magnitude appears to be a property of the particular path, the distribution in magnitude for each path was investigated. In order to accomplish this, the data for each path were sorted according to the size of the amplitude (ΔA) and phase ($\Delta\phi$) changes. Figure 7 contains eight graphs showing the distribution of ΔA for each path, while Figure 8 shows the corresponding distributions of $\Delta\phi$. Most of these graphs have similar envelopes resembling lognormal probability distributions [*Sachs*, 1984]. The distinctive features of these distributions are relatively few events near zero, the number of events rising rapidly to a peak, and then tapering off slowly as the magnitude of the event increases. The location of the peak and the width of the distribution depends upon the path, but the same general shape is apparent in most of the plots.

The fact that all of the plots have similar envelopes suggests that this shape may be a physical property of the Trimpi effect.

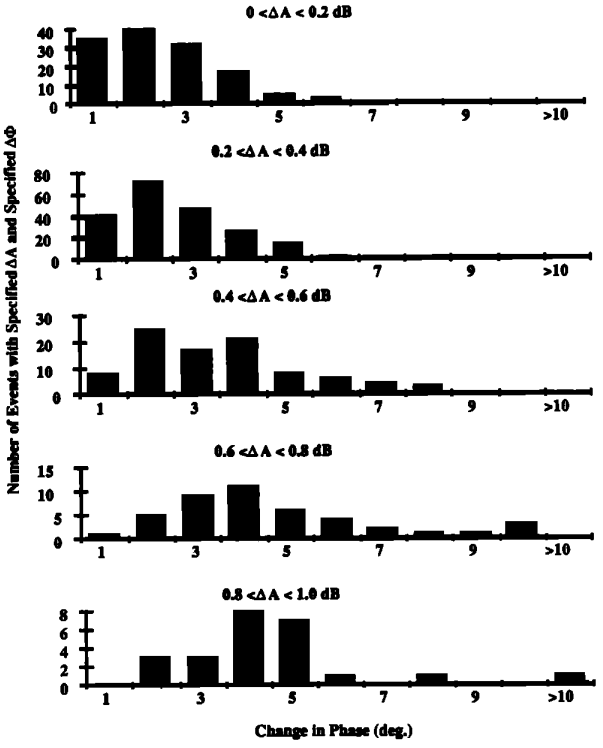

Fig. 6. Each panel contains a different range of ΔA (labeled amplitude and measured in dB), from smallest at the top to largest at the bottom. For each range, the distribution of $\Delta\phi$ is shown. All data are from the NPM to Palmer path.

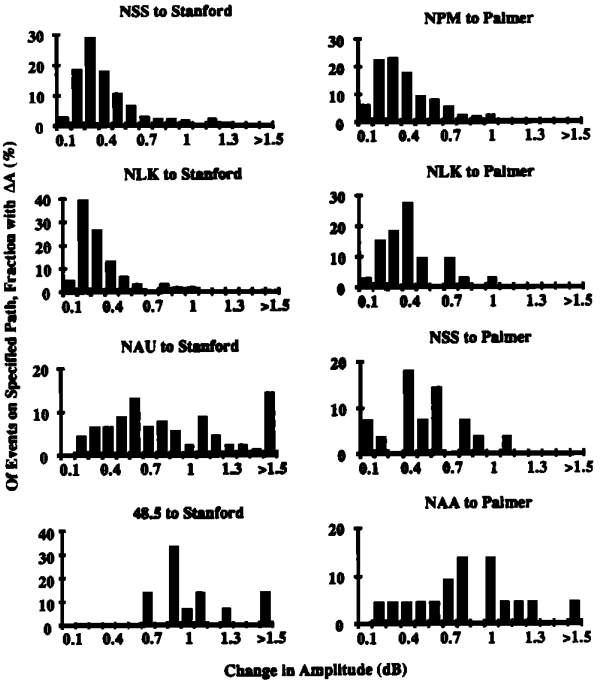

Fig. 7. For each of the eight paths, histograms show the percent of events in different ΔA ranges. Only nonzero events are shown.

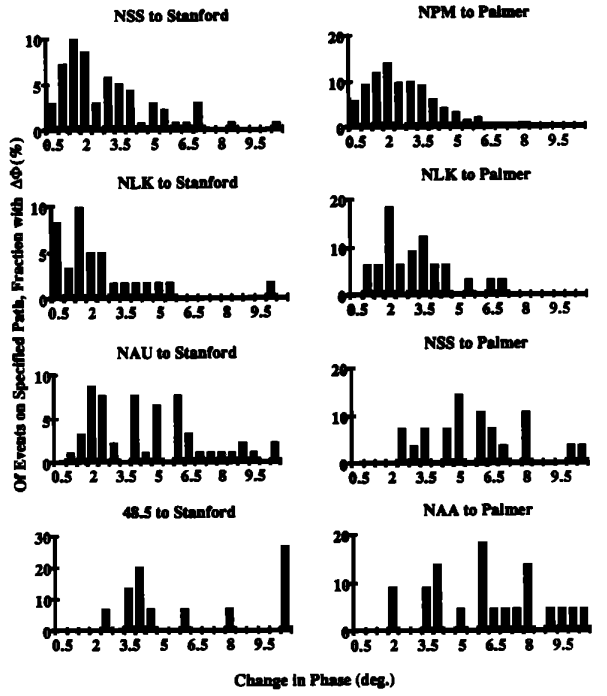

Fig. 8. For each of the eight paths, histograms show the percent of events in different $\Delta\phi$ ranges. Only nonzero events are shown.

Many lightning parameters, including return-stroke current have been found to exhibit lognormal distributions [*Uman*, 1987]. *Inan and Carpenter* [1986] have reported a correlation between event magnitude and associated whistler intensity, so it would be interesting to establish whether whistler intensities exhibit a similar distribution. Since the width of the distribution ($\Delta\phi_m, \Delta A_m$) is a property of the path, this is probably determined by the particular waveguide properties of that path (e.g., frequency, path length, location of the receiver with respect to the minima and maxima along the path, conductivity variation, and roughness of the Earth's surface along the path) and by the number of propagating modes that are dominant for that path.

5. Significance of ΔA Versus $\Delta\phi$ Properties

A typical profile of nighttime ambient electron density [*Poulsen et al.*, 1990] versus altitude for the lower ionosphere is shown in Figure 9. Also shown is the excess electron density profile generated by a 0.2 s burst of isotropic 300-keV electrons at a flux level of 10^{-3}ergs/ cm^{-2}- s^{-1}, calculated in accordance with ion-pair production rates given by *Rees* [1969]. Even this simplified monoenergetic burst has the excess electrons distributed over a range of altitudes, and an actual electron precipitation event will have a more complicated profile that depends upon electron energy distribution, pitch angle distribution, and ionospheric properties. A number of different simplified models for the consequences of this perturbation have been utilized to explain specific observations. These models are useful for a conceptual understanding of the Trimpi phenomenon, but applying them to this larger set of data brings out their limitations. In the following we discuss our results in the context of these various models.

Reflection Height Lowering Model

The simplest model, called Reflection Height Lowering (RHL), makes several simplifying assumptions about the Earth-ionosphere waveguide and the nature of the ionospheric disturbance. The first assumption is that of horizontal symmetry in all features perpendicular to the direction of propagation. This assumption reduces the model to two dimensions, one horizontal direction along the line between the transmitter and receiver, and one vertical dimension between the Earth's surface and the ionosphere. This simplification is equivalent to assuming that all disturbances in the ionosphere occur right on the signal path, between receiver and transmitter, and extend far off the path in the perpendicular direction. A second simplification is that reflection occurs at a specific altitude determined by the local electron concentration and electron collision frequency. If the precipitation event causes an increase in the electron concentration in the vicinity of this altitude, the altitude at which the reflection occurs is lowered (typically by 1-2 km [*Inan et al.*, 1985]).

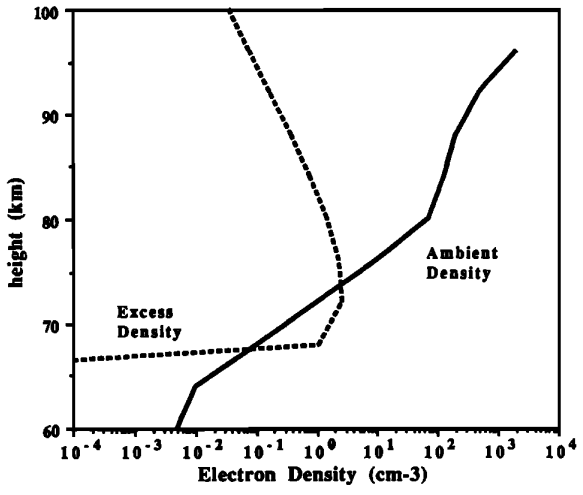

Fig. 9. The typical electron density of the nighttime lower ionosphere [*Poulsen et al.* 1990] is shown along with the excess electron profile generated by a burst of 300-keV electrons (computed from *Rees* [1969]). An actual precipitation event would be distributed in electron energy and pitch angle, and so would yield an excess electron profile that is even more distributed in altitude.

When the subionospheric wave reflects at a lower altitude, the total path length from transmitter to receiver is shortened, which appears as a slight decrease in propagation time to the receiver. Thus a lowering of the reflection height appears as an advancement in the phase of the received signal. The fact that nearly all paths observed exhibit a strong preference for phase advancement is consistent with this simple mechanism. Along with RHL, the excess electrons caused by precipitation would lead to an increase in the VLF absorption coefficient in the vicinity of the reflection height, so events would be likely to exhibit simultaneous phase advancement and amplitude attenuation. However, some paths frequently exhibit amplitude enhancement, and many have occasional phase retardation, which cannot be explained by simple RHL.

Since the Earth-ionosphere waveguide supports multiple waveguide modes, it usually is not sufficient to evaluate the effect of RHL on a single-mode signal. Instead the effect on the vector sum of a number of different propagating modes must be considered. The attenuation rate for a path depends upon the mode and the surface of the waveguide, so the selection of which modes and how many of them to consider can be complicated [*Tolstoy et al.*, 1986]. For long paths over seawater, such as NPM-PA, a single propagating mode is generally considered adequate [*Inan and Carpenter*, 1987], and indeed, this path exhibits almost entirely phase advancement and amplitude attenuation. There is, however, more to the waveguide than this simple picture, since the NLK-PA path, which is very similar to NPM-PA (except that NLK-PA crosses the western United States before entering the ocean), has a strong preference for amplitude enhancement.

When multiple modes are considered, a wide variety of amplitude and phase changes can result [*Tolstoy et al.*, 1986]. Using the basic assumption of RHL, that each mode experiences a phase advance, large amplitude changes (either enhancement or attenuation), and large phase changes (either advancement or retardation) could occur when several modes are combined in a destructive manner, as illustrated in Figure 10. Under these conditions, each mode experiences a small change, but small changes in the phase of the modes can dramatically change the degree to which they interfere and thus dramatically change the relative magnitude and phase of the received sum. This modal interference situation is consistent with the fact that the path that exhibits

Fig. 10. When two strong signals propagating in different modes (represented by vectors A and B) combine in a destructive manner (i.e., a small difference between large values), small changes in each mode (from the original grey vector to the new black vector) can result in large phase changes and large relative amplitude changes in the sum.

the widest variations in ΔA and $\Delta\phi$, 48.5-SU, is also the one with the high likelihood of phase retardation. However, we note that multiple mode interference would also be expected to affect the NLK-SU path, entirely land-based and the shortest path, and yet this path has small events (similar in distribution to NPM-PA), only attenuation, and more phase advancement than retardation: all properties similar to those of single-mode paths.

A single-mode picture would suggest that there should be a direct correlation between the magnitude of $\Delta\phi$ and the magnitude of ΔA; the more electrons that are added to the ionospheric, the more the reflection height should lower, and the more absorption that should occur near the reflection height. Such a direct correlation is not apparent in the data. When multiple modes are involved, the opposite should be true. If the modes interfere destructively, then large phase changes should occur when the net change signal vector is perpendicular to the original sum signal vector, and under these circumstances the amplitude change would be small. Similarly, when the net change is in phase with the original sum, large amplitude changes would occur with small phase changes. This would imply that the scatter plots (Figures 4 and 5) should contain concentrations of large events near the axes, and few large events off of the axes. Such a pattern is not apparent in any of the scatter plots.

Thus while reflection height lowering is a good method of visualizing the ionospheric disturbance and its effects on the subionospheric signal, it does not adequately describe the underlying physics and cannot be successfully applied to all paths, even when multiple propagating modes are considered.

Off-Axis Scattering Model

Rather than lowering the reflection height in a region along the signal path, the mechanism for signal disturbance might be one of Off-Axis Scattering (OAS) [*Dowden and Adams*, 1988]. The excess ionization might form a small diffracting bubble (or "stalactite") on the bottom of the ionosphere displaced from the great circle path of the propagating signal. This bubble would then act as a scattering center deflecting part of the transmitted signal to the receiver. Thus when the perturbation occurs, a second signal component deflected to the receiver would be received in addition to the original signal. The vector sum of these two components would then appear as the perturbed signal.

This concept may apply under certain circumstances, but it does not agree with most of the results found here. Assuming, as Dowden and Adams do, that scattering is equally effective at a range of distances from the path, phase advancement and retardation as well as amplitude attenuation and enhancement should be equally common and should not depend upon the particular path being studied, in contradiction with the findings reported here. In particular, the NPM-PA path, a simple single-mode path, has almost entirely phase advancement and amplitude attenuation, not the even polarity distribution predicted by OAS. In addition, the variation in event magnitude (ΔA_m and $\Delta\phi_m$) with path would not be expected with off-axis scattering, where the magnitude is simply a function of the geometry. Finally, as with the multiple-mode discussion above, simple vector addition indicates that large phase changes occur when the scattered vector is perpendicular to the original signal vector, implying no amplitude change, and large amplitude changes occur when the vectors are parallel, implying no phase change. Thus the scatter plots (Figures 4 and 5) should contain concentrations of larger events near the axes, with relatively few of the large events far from the axes of the plot. This expectation also does not agree with the observations. Thus while off-axis scattering is an interesting concept and may be applicable under certain conditions, it is not sufficient for obtaining a general understanding of localized ionospheric disturbances and their effects on subionospheric signals.

Waveguide Mode Propagation Models

Detailed computer models of the Earth-ionosphere waveguide have been used to analyze the effect of ionospheric disturbances on signal propagation [*Tolstoy et al.*, 1982; 1986]. These models consider the structure of the Earth's surface along the path, allow for variation in ionospheric electron concentration with height and position, and analyze multiple propagating modes. Tolstoy obtained some interesting results such as on NPM-PA "small amplitude decreases could be produced," while on NLK-PA "...generally produce small increases in the NLK signal amplitude ...small decreases can also occur." Both of these conclusions agree with the observations reported here, but it should be noted that Tolstoy's analysis of the NLK path assumed a transmitter frequency of 18.6 kHz, while the transmitter had switched to 24.8 kHz before any of the current data were collected.

Poulsen et al. [1990] have started the development of a new three-dimensional waveguide model. This model uses analytical expressions, provided by *Wait and Spies* [1964], for the wave fields of each propagating mode, and utilizes perturbation theory to analyze the effect of a localized ionospheric disturbance. The complex refractive index both for the background ionosphere and for the disturbed region are determined numerically, for each mode, based upon ionospheric properties such as electron profile, and other waveguide properties such as earth conductivity [*Morfitt and Shellman*, 1976]. This new formulation allows for the possibility of the perturbation not being on the great circle path and of the waveguide not being uniform in the horizontal direction perpendicular to the path. Instead, the disturbance is allowed to occur anywhere in the lower ionosphere, in the vicinity of the path. Although multiple modes have not yet been analyzed with this model, preliminary results indicate that phase advances are common for disturbed regions near the path, as expected. Also, the location of the disturbance, both its position along the path and its offset from the path, can cause significant variation in the magnitude and polarity of both ΔA and $\Delta\phi$. Ranges of both ΔA and $\Delta\phi$ magnitude found using this waveguide analysis agree with the observations for simple paths such as NPM-PA [*Poulsen et al.*, 1990].

6. INDEPENDENCE OF HIGH TIME RESOLUTION EVENT SIGNATURES

To further investigate the apparent independence between the amplitude and simultaneous phase events, arbitrarily selected events were examined at higher time resolution. Figure 11 shows a typical event where the amplitude and phase recoveries appear quite similar in shape. Figure 12 is a similar plot showing events observed on the NPM to Palmer path. Although recoveries have not yet been studied in detail on this data set, in this event, and others observed, the phase recovery time appears to be substantially longer than the amplitude recovery.

Figure 13 shows another event with very different amplitude and phase signatures. In this event the onset of the phase change appears to be much slower than the onset of the simultaneous amplitude change, and the phase may start to advance before the beginning of the amplitude change. Although the amplitude signature of this event is typical of a Trimpi event, the phase signature is so unusual that a different, as yet undetermined, mechanism may be involved. Events with these anomalous signatures are cu-

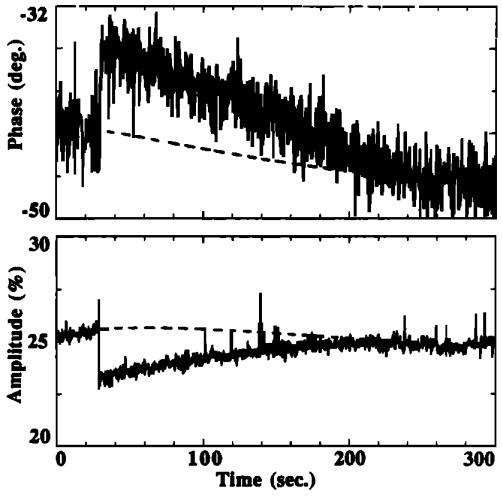

Fig. 11. The NSS transmitter signal phase (Top) observed at Stanford as a function of time, and the simultaneous amplitude (bottom). Dashed lines represent the interpolated levels if no event had occurred. Both amplitude and phase have similar sharp onsets and similar recoveries to pre-event levels. The data shown was time averaged over 0.32 s. The plot starts at 02:25 UT on March 15, 1987.

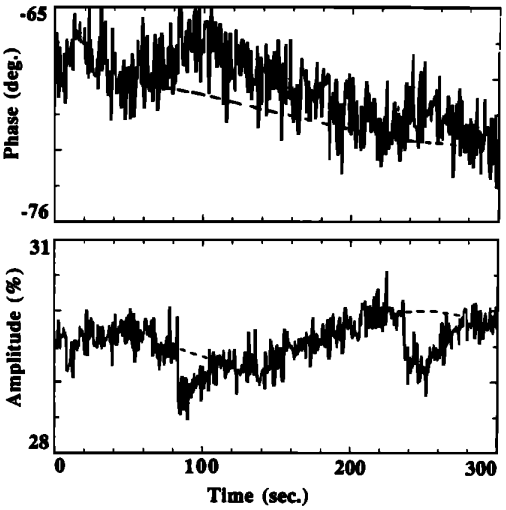

Fig. 13. The amplitude and phase of the NPM transmitter signal are shown as observed at Palmer Station. In this event, the amplitude has the characteristic rapid onset and slow recovery, but the simultaneous phase measurement shows a much slower onset. The phase also may start to advance before the amplitude change begins. The data was time-averaged over 0.64 s. The plot starts at 09:15 UT on May 5, 1988.

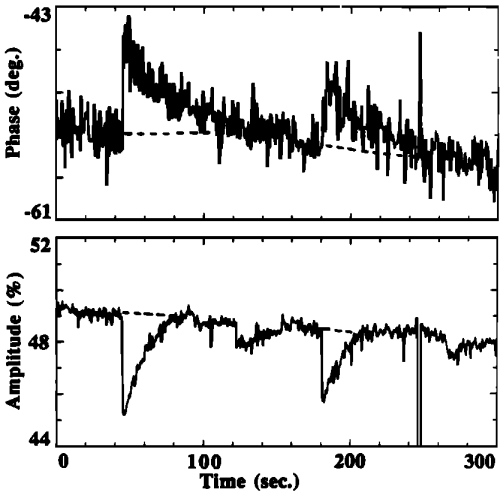

Fig. 12. The amplitude and phase of the NPM transmitter signal are shown as observed at Palmer Station. Both events shown here have substantially faster amplitude recoveries than phase recoveries. The dashed lines represent the interpolated levels if no event had occurred. The data was time averaged over 0.64 s. The plot starts at 06:37 UT on May 4, 1988.

rious, but they occur only rarely ($\sim$ 1% of events analyzed) and would not affect the statistical analyses presented here.

These observations imply that the disturbance in the ionosphere affects the amplitude and phase of the signal independently. While acknowledging that the excess ionization is distributed in altitude, most previous discussions using simple models have treated the change in the ionosphere as a patch of excess ionization at one altitude, typically near the nighttime reflection height. The effect of the disturbance then becomes essentially a change in geometry, that is, the reflection height is lowered, the waveguide has a depression, or an additional scattering center appears. If this single geometric change occurs and then gradually recovers to normal, the amplitude and phase of the perturbation would be expected to have similar time signatures. The results reported here indicate that not only are the magnitudes of amplitude and phase events independent, but also that the time signatures are often independent too.

The most likely explanation for this independence lies in the fact that the excess ionization is actually distributed over a range of altitudes in the lower ionosphere. Collision frequency decreases with increasing altitude in this region and so does excess ion recombination rate [*Gledhill*, 1986]. Thus the excess electrons generated higher up would be expected to persist longer than those lower down. Since significant absorption occurs below the reflection height, where the recombination rate is higher, it would not be surprising that amplitude changes recover quickly, while phase changes, which are influenced by electrons higher up, recover more slowly.

The waveguide propagation models [*Tolstoy et al.*, 1986; *Poulsen et al.*, 1990] have utilized a disturbance distributed in altitude, and so more accurately reflect the range and independence of ΔA and $\Delta\phi$ found. In particular, *Poulsen et. al.*, [1990] have shown that by varying the energy of the precipitated electrons, and therefore the altitude of the excess ionization, a wide range of ΔA versus $\Delta\phi$ distributions can be obtained. Thus a range of precipitation events, with a range of electron energies would be expected to produce a scatter plot of ΔA versus $\Delta\phi$ with a fairly uniform distribution, as has been reported here. None of these models currently simulates the time evolution of ionospheric disturbances, so event recoveries have not been investigated, and the faster amplitude recoveries observed here have not been confirmed with computer simulations.

7. Summary and Conclusions

The existing simple models for the mechanism of the Trimpi effect are useful primarily as conceptual and qualitative explanations of the phenomenon. They may even accurately describe some individual events but cannot be generalized to explain the new patterns and features of the Trimpi effect revealed in this anal-

ysis. Instead, these new features provide an empirical framework that will guide the evolution of the more sophisticated models that are currently being developed.

Among the important new features found, with which new models of the ionospheric disturbance and its effects on VLF signals must be consistent, are the following:

1. Amplitude changes are evenly distributed, overall, between enhancement and attenuation, but some individual paths have strong preferences for one or the other.

2. Phase changes show a different character in that almost all paths show a strong preference for phase advancement; phase retardation does occur, but it is rare.

3. The range in size of amplitude and phase events varies between paths, but it is relatively constant with time for a given path.

4. The magnitudes of simultaneous amplitude and phase changes are correlated, but only weakly.

Preliminary analysis of the time signatures of events has also shown that in many events with simultaneous amplitude and phase changes on a given signal, the two changes have different behavior with time. This suggests that not only are the occurrence rate and size of simultaneous amplitude and phase events independent, but also that the time signatures are independent too. This independence implies that it is inadequate to treat the ionosphere as an abrupt waveguide boundary with a perturbation in the altitude of the boundary. Instead, the ionosphere must be treated as a continuous, varying medium, forming a gradual boundary, with absorption, reflection, and transmission properties changing with altitude. In addition, the disturbance in the ionosphere, caused by enhanced ionization from the precipitating electrons, must be treated as a three-dimensional change in this medium, distributed not only in horizontal extent, but also in altitude. The difference in recovery times for amplitude and phase may then be indicative of the altitude dependence of the ion recombination rate.

Acknowledgments. We thank our colleagues in the STAR Laboratory for useful discussions and D. Shafer and W. Burgess for their excellent field work at Palmer Station. We also thank Zheng Xu for her typesetting of the manuscript. This research was sponsored by the National Science Foundation under grant DPP-8611623 from the Division of Polar Programs and under grants ATM-8415464 and ATM-8804273 from the Division of Atmospheric Sciences.

The Editor thanks T. J. Rosenberg and another referee for their assistance in evaluating this paper

REFERENCES

Armstrong, W. C., Recent advances from studies of the Trimpi effect, *Antarctic Journal, 18*, 281, 1983.

Burgess, W. C., and U. S. Inan, Simultaneous disturbance of conjugate ionospheric regions in association with individual lightning flashes, *Geophys. Res. Lett., 17*, 259, 1990.

Carpenter, D. L., and U. S. Inan, Seasonal, latitudinal and diurnal distributions of whistler-induced electron precipitation events, *J. Geophys. Res., 92*, 3492, 1987.

Carpenter, D. L., U. S. Inan, M. L. Trimpi, R. A. Helliwell, and J. P. Katsufrakis, Perturbations of subionospheric LF and MF signals due to whistler-induced electron precipitation bursts, *J. Geophys. Res., 89*, 9857, 1984.

Carpenter, D. L., U. S. Inan, E. W. Paschal, and A. J. Smith, A new VLF method for studying burst precipitation near the plasmapause, *J. Geophys. Res., 90*, 4383, 1985.

Chang, H. C., and U. S. Inan, Test particle modeling of wave-induced energetic electron precipitation, *J. Geophys. Res., 90*, 6409, 1985.

Davies, K., *Ionospheric Radio Propagation*, U. S. Government Printing Office, Washington D. C., 1965.

Dowden, R. L., and C. D. D. Adams, Phase and amplitude perturbations on subionospheric signals explained in terms of echoes from lightning-induced electron precipitation ionization patches, *J. Geophys. Res., 93*, 11,543, 1988.

Dowden, R. L., and C. D. D. Adams, Phase and amplitude perturbations on the NWC signal at Dunedin from lightning-induced electron precipitation, *J. Geophys. Res., 94*, 497, 1989.

Gledhill, J. A., The effective recombination coefficient of electrons in the ionosphere between 50 and 150 km, *Radio Sci., 21*, 399, 1986.

Helliwell, R. A., J. P. Katsufrakis, and M. L. Trimpi, Whistler-induced amplitude perturbation in VLF propagation, *J. Geophys. Res., 78*, 4679, 1973.

Hurren, P. J., A. J. Smith, D. L. Carpenter, and U. S. Inan, Burst precipitation-induced perturbations on multiple VLF propagation paths in Antarctica, *Ann. Geophys., 4*, 311, 1986.

Inan, U. S., and D. L. Carpenter, On the correlation of whistlers and associated subionospheric VLF/LF perturbations, *J. Geophys. Res., 91*, 3106, 1986.

Inan, U. S., and D. L. Carpenter, Lightning-induced electron precipitation events observe at L≈2.4 as phase and amplitude perturbations on subionospheric VLF signals, *J. Geophys. Res., 92*, 3293, 1987.

Inan, U. S., D. L. Carpenter, R. A. Helliwell, and J. P. Katsufrakis, Subionospheric VLF/LF phase perturbations produced by lightning-whistler induced particle precipitation, *J. Geophys. Res., 90*, 7457, 1985.

Inan, U. S., W. C. Burgess,, T. G. Wolf, D. C. Shafer, and R. E. Orville, Lightning-associated precipitation of MeV electrons from the inner radiation belt, *Geophys. Res. Lett., 15*, 172, 1988*a*.

Inan U. S., T. G. Wolf, and D. L. Carpenter, Geographic distribution of lightning-induced electron precipitation observed as VLF/LF perturbation events, *J. Geophys. Res., 93*, 9841, 1988*b*.

Inan U. S., D. C. Shafer, W. Y. Yip, and R. E. Orville, Subionospheric VLF signatures of nighttime D-region perturbations in the vicnity of lightning discharges, *J. Geophys. Res., 93*, 11,455, 1988*c*.

Inan, U. S., F. A. Knifsend, and J. V. Rodriguez, Subionospheric VLF "imaging" of lightning-induced electron precipitation from the magnetosphere, *Eos, Trans. AGU, 69*, 1392, 1988*d*.

Inan, U. S., M. Walt, H. D. Voss, and W. L. Imhof, Energy spectra and pitch angle distributions of lightning-induced electron precipitation: Analysis of an event observed on the S81-1(SEEP) satellite, *J. Geophys. Res., 94*, 1379, 1989.

Inan U. S., F. A. Knifsend, and J. Oh, Subionospheric VLF "imaging" of lightning-induced electron precipitation from the magnetosphere, *J. Geophys. Res., 95*, 17,217, 1990.

Lohrey, B., and A. B. Kaiser, Whistler-induced anomalies in VLF propagation, *J. Geophys. Res., 84*, 5122, 1979.

Morfitt, D. G., and C. H. Shellman, MODESRCH, An improved computer program for obtaining ELF/VLF/LF mode constants in an earth-ionosphere waveguide, *Interim Rep. No. 77T*, Propagation Technol. Div., Nav. Electron. Lab. Cent., San Diego, Calif., 1976.

Poulsen, W. L., T. F. Bell and U. S. Inan, 3-D modeling of subionospheric VLF propagation in the presence of localized D-region perturbations associated with lightning, *J. Geophys. Res., 95*, 2355, 1990.

Rees, M. H., Auroral electrons, *Space Sci. Rev., 10*, 413, 1969.

Sachs, L., *Applied Statistics*, Springer-Verlag, New York, 1984.

Tolstoy, A., T. J. Rosenberg, and D. L. Carpenter, The influence of localized precipitation-induced D-region ionization enhancements on subionospheric VLF propagation, *Geophys. Res. Lett., 9*, 563, 1982.

Tolstoy, A., T. J. Rosenberg, U. S. Inan, and D. L. Carpenter, Model predictions of subionospheric VLF signal perturbations resulting from localized, electron precipitation-induced ionization enhancement regions, *J. Geophys. Res., 91*, 13,473, 1986.

Uman, M. A., *The Lightning Discharge*, Academic, San Diego, Calif., 1987.

Voss, H. D., et al., Lightning-induced electron precipitation, *Nature, 312*, 740, 1984.

Wait, J. R., and K. P. Spies, Characteristics of the earth-ionosphere waveguide for VLF radio waves, *NBS Tech. Note U.S., 300*, 1964.

Wolf, T. G., Remote sensing of ionospheric effects associated with lightning using very low frequency radio signals, Ph.D Thesis, Stanford Univ., Stanford, Calif., 1990.

Yip, W. Y., U. S. Inan, and R. E. Orville, On the spatial relationship between lightning discharges and propagation paths of perturbed subionospheric VLF/LF signals, *J. Geophys. Res.*, (in press) 1990.

T. G. Wolf and U. S. Inan, Space, Telecommunications And Radioscience Laboratory, Department of Electrical Engineering/SEL, Stanford University, Stanford, CA 94305.

(Received March 19, 1990;
revised June 14, 1990;
accepted July 17, 1990.)